Journal of Physics D: Applied Physics

PAPER

Quantum dot based mid-infrared photodetector enhanced by a hybrid metal-dielectric optical antenna

To cite this article: Andrew Yakimov *et al* 2020 *J. Phys. D: Appl. Phys.* **53** 335105

IOP Publishing Journal of Physics D: Applied Physics
J. Phys. D: Appl. Phys. **53** (2020) 335105 (7pp) https://doi.org/10.1088/1361-6463/ab84a7

Quantum dot based mid-infrared photodetector enhanced by a hybrid metal-dielectric optical antenna

Andrew Yakimov[1,2], Victor Kirienko[1], Aleksei Bloshkin[1,3], Anatolii Dvurechenskii[1,3] and Dmitrii Utkin[1,3]

[1] Rzhanov Institute of Semiconductor Physics, Siberian Branch of the Russian Academy of Science, 630090 Novosibirsk, Russian
[2] Tomsk State University, 634050 Tomsk, Russian
[3] Novosibirsk State University, 630090 Novosibirsk, Russian

E-mail: yakimov@isp.nsc.ru

Received 10 January 2020, revised 4 March 2020
Accepted for publication 30 March 2020
Published 8 June 2020

Abstract

Surface plasmon waves and Rayleigh anomaly are characteristic optical phenomena exhibited by periodic subwavelength grating structures. In this paper, a hybrid metal-dielectric metasurface is proposed to improve the photoresponse of Ge/Si quantum dot infrared photodetectors (QDIPs) with limited absorption layer thickness. The composite metasurface consists of a regular array of silicon pillars. The pillars protrude through subwavelength holes in a perforated gold film on the detector top. We demonstrate that by combining effects of dielectric and plasmonic metal components, the QDIP photoresponse can be significantly improved compared to case when all-dielectric and metal gratings work alone. We observe about four times photoresponse enhancement with the hybrid metasurface device relative to a common plasmonic design with a two-dimensional metal hole array. Compared with a bare QDIP, the peak responsivity of the hybrid detector at a wavelength of 4.4 μm is increased by a factor of 15. The enhanced sensitivity is supposed to arise from coupling of the surface plasmon resonance and diffractive effect related to the Rayleigh anomaly.

Keywords: quantum dots, infrared photodetection, surface plasmons, near-field enhancement

(Some figures may appear in colour only in the online journal)

1. Introduction

Quantum dot (QD) infrared (IR) photodetectors (QDIPs) have attracted significant research interest in recent years, primarily due to their low dark current, high internal gain, and tunability of wavelength detection originating from the discretization of energy spectrum. Despite the aforementioned superior features of QDs, a limitation in conventional QDIPs is that the absorbance of mid-IR radiation is weak, which results from the low density of states coupled to the dots and from the limited QD absorption layer thickness. Recently, photodetection improvement was observed for mid-IR InAs/(In)GaAs [1–5] and Ge/Si(Ge) [6–8] QDIPs integrated with periodic plasmonic structures to convert the incident electromagnetic radiation into the surface plasmons (SPs). Metallic films perforated with two-dimensional subwavelength hole arrays (2DHAs) were used as the plasmonic couplers. SP occurs at the resonance wavelength of $\lambda_{SP} = [a\varepsilon_m\varepsilon_d/(\varepsilon_m + \varepsilon_d)]^{1/2}$, when the collective charge oscillations on the surface of a metal grating are excited. Here, a is the array periodicity, ε_m and ε_d are the relative permittivities of the metal and dielectric, respectively. The excitation of SPs offers an effective surface light trapping, enhancement of local field intensities, and thus interaction with the optically thin QD active region.

The generation of SPs was originally proposed to explain the extraordinary optical transmission (EOT) effect in 2DHA metal films [9–11]. This seems quite natural since the surface plasmons are responsible for a type of grating anomaly at visible or near-infrared frequencies. However, at long wavelengths (far-IR, terahertz or microwave), metals such as

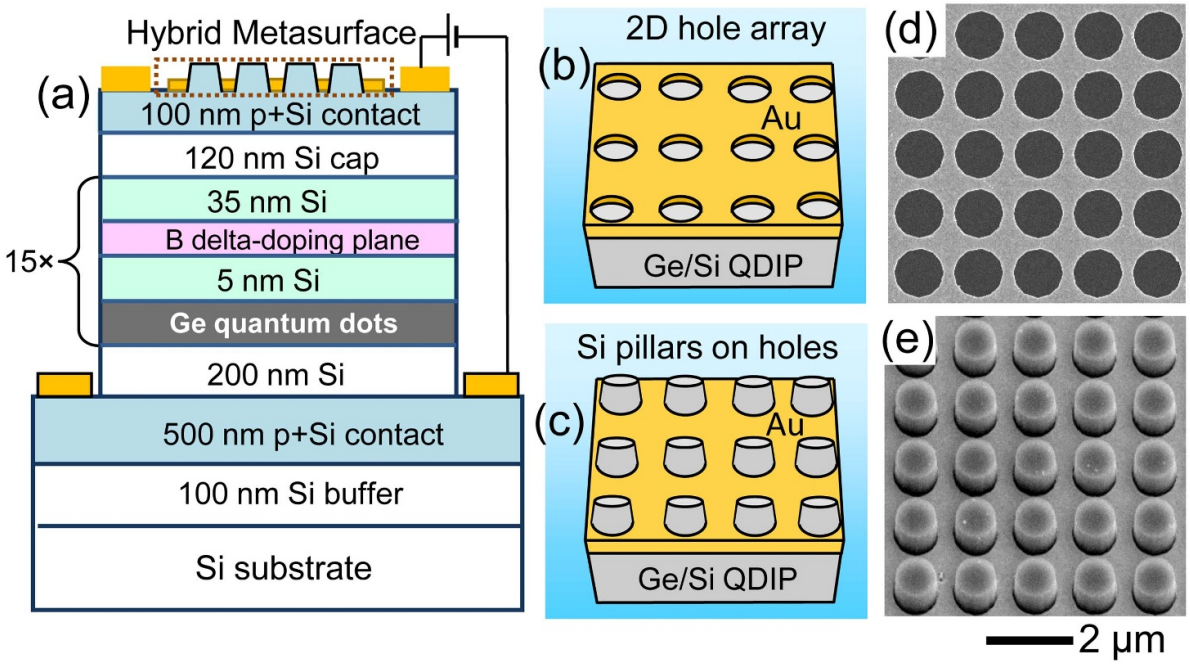

Figure 1. (a) Layer sequence of the 15-period Ge/Si QDIP enhanced with the top hybrid metasurface. (b), (c) Schematic illustrations of metasurfaces that contain (b) a regular 2D metal hole array and (c) a periodic array of Si micropillars mounted on holes of the 2DHA. (d), (e) Zoom-in scanning electron microscopy (SEM) images of the investigated metasurfaces on top of the Ge/Si QDIPs: (d) the 2D hole array in a gold film (plan view), (e) the array of Si micropillars protruding through the holes of the perforated gold film (tilted view). In all devices, the array periodicity is 1.3 μm.

gold and silver behave like perfect electric conductors with a zero skin depth and do not support conventional SP modes [12, 13]. Nevertheless, the same metals textured with subwavelength holes can give rise to guided leaky surface waves (usually termed as spoof plasmons) that have almost perfect analogy to the natural SPs [14–16], and mimic all aspects of their behavior at much shorter wavelengths. The question of whether the mid-wave ($3-5$ μm) plasmons are real or designed is currently being debated [17] and is beyond the scope of this paper. In what follows, we name the observed mid-IR bound surface excitations as SPs, although they can represent the spoof SPs. This assumption does not undermine the final conclusions.

Another grating phenomenon is the Rayleigh anomaly (RA), a diffraction effect, which is associated with light being diffracted at an angle parallel to the metal surface [18, 19]. The RA occurs at the wavelength given by $\lambda_{RA} = a\varepsilon_d^{1/2}$. At mid-IR frequencies, the absolute value of the real permittivity of noble metals is much larger than that of typical dielectrics and $\lambda_{RA} \simeq \lambda_{SP}$. Therefore, the interplay between RAs and SPs may strongly affect the optical properties of subwavelength metal gratings [20, 21]. Many studies are dedicated to the problem of optical anomalies, focusing mainly on the case of metallic gratings. In the meantime, there is an increasing interest in resonant all-dielectric elements, as they offer a low-loss alternative to plasmonic structures [22–28]. It has been recently demonstrated that composite photonic-plasmonic hybrid structures form a novel platform for functional nanophotonics as they combine the advantages of both the dielectric and metal metasurfaces [29–33]. Investigations of EOT phenomena in gold films embedding 2D arrays of polymeric nanopillars [34], GaAs micro-domes [35], and SU-8 micro-lens [36] revealed the enhanced transmission and broadening via coupling of scattered fields into the holes of plasmonic film. A recent topical review on IR detectors enhanced by metallo-dielectric structures can be found in [37].

In our work, a hybrid metasurface composed of Si micro-domes protruding through subwavelength holes of a periodically perforated gold film is proposed to improve the photoresponse of mid-IR Ge/Si QDIPs. The metasurface is integrated on top of the detector active region (figure 1(a)) and produces a very strong RA, with near-field intensity higher than that of the SP. Ge/Si QDIP with a composite metal-dielectric metasurface exhibits a fourfold photoresponse enhancement at $\lambda = 4.4$ μm, as compared to a common plasmonic design with 2DHA.

2. Experimental details

The Ge/Si QD samples were grown using a Riber SIVA21 molecular beam epitaxy (MBE) system. A 0.5 μm boron-doped p^+-Si contact layer ($p = 2 \times 10^{18}$ cm^{-3}) was first grown on a Si (100) wafer (figure 1(a)). The active region of QDIPs was composed of 15 stacks of Ge quantum dots separated by 40 nm Si barriers and was sandwiched in between the 200 nm thick undoped buffer and 120 nm thick cap Si layers. Each Ge QD layer consisted of a nominal Ge thickness of about 0.8 nm and formed at 500 °C with a rate of 0.05 Å/s by self-assembling in the Stranski–Krastanov growth mode. Cross-sectional images obtained by transmission electron microscopy [38, 39] and scanning tunneling microscopy

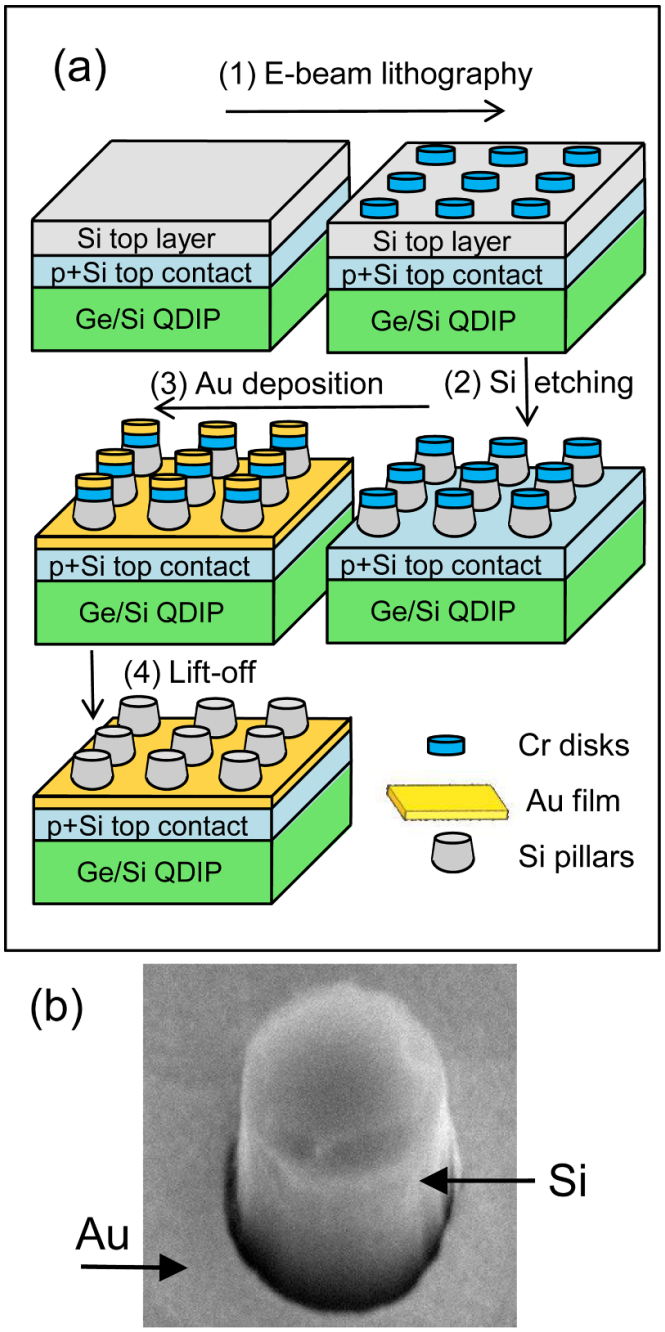

Figure 2. (a) Schematic presentation of the processing steps in the fabrication of the silicon pillars embedded in the 2D metal grating. (b) The high resolution SEM image of the metal edge near the pillar. The Si pillars have an almost cylindrical shape with a typical base diameter of ~1.0 μm and a height of 0.5 μm.

experiments with uncapped samples [38, 40, 41] demonstrated that the Ge dots have the form of hut clusters bounded by 105 facets with a typical base length of 11 ± 2 nm, a height of about 2 nm, and an areal density of $\simeq 10^{11}$ cm^{-2}.

The p-type remote doping of the dots was achieved with a boron δ-doping laye,r inserted 5 nm above each dot layer. The areal doping density was 6×10^{11} cm^{-2}. Finally, a boron doped 100-nm-thick p^+-Si top contact layer (10^{19} cm^{-3}) was grown. In certain cases, an undoped 500-nm-thick Si layer was deposited on the top contact layer for further fabrication of the devices with Si micro-domes on their surface. After the MBE growth, the wafers were processed into 700 μm diameter circular mesa-shaped QDIPs with top and bottom gold electrodes (figure 1(a)). The growth conditions are similar to the QDIPs reported before [8].

In this work, all measurements were performed at a temperature of 78 K. The samples were mounted in a cold finger inside a Specac cryostat with ZnSe windows. The devices under test were biased at -1 V. The incident nonpolarized IR light iilluminated detectors from their top (pillar) side. The photoresponse and transmittance spectra were recorded using a Bruker Vertex 70 Fourier transform infrared spectrometer with a spectral resolution of 10 cm^{-1} along with a Stanford SR570 low noise current preamplifier. The photocurrent spectra were calibrated with a deuterated L-alanine doped triglycine sulfate (DLaTGS) detector. It is necessary to note that special caution must be taken when measuring the photocurrent spectra by using a FTIR technique. Since the samples in this system are simultaneously exposed to a wide range of photon energies, the spectra may display additional transitions due to two-photon processes [42]. A 2 mm thick Si wafer serving as filter was introduced in front of the samples to eliminate the photons, which may cause band-to-band transitions in the Si layers.

Four different device types were fabricated. The first one is a reference QDIP with an as-grown QDIP surface. On top of the second QDIP, we fabricate a metallic 2DHA plasmonic structure by the deposition of a 50 nm thick Au film and formation of a periodic lattice of circular holes using the electron-beam lithography, e-beam metal deposition and lift-off processing (figure 1(b)). The 2DHA covers an area of 500 μm in diameter, and has the square lattice symmetry with lattice constant of 1.3 μm and hole diameter of 1 μm (figure 1(d)). The perforated gold film was designed to excite the first-order SP mode around the responsivity maximum of the bare detector (4.3–4.5 μm). The third device contains a hybrid metasurface, which is composed of both the periodically perforated gold film and Si micropillars mounted on each hole of the 2DHA (figure 1(c)). The Si pillars have an almost cylindrical shape with a typical base diameter of ~1.0 μm and a height of 0.5 μm (figure 1(e)). The fourth sample is a heterostructure with a periodic array of Si micropillars on top of the detector without the perforated gold film. The array periodicity is the same as that of the 2DHA (1.3 μm).

The fabrication process of Si pillars is shematically illustrated in figure 2(a). (1) A square array of Cr disks is formed on top of the QDIPs using the electron-beam lithography, e-beam metal deposition and lift-off techniques. (2) A reactive-ion etch is performed through the Cr disks down to the buried p^+-Si layer. The process left behind a square array of Si pillars with the Cr caps on their top. (3) A thin Ti layer (5 nm), used to improve the metal adhesion to the Si, and a thicker Au layer (50 nm) are then deposited. (4) A lift-off step using the sacrificial Cr slabs removes the Au caps from the top of Si pillars leaving behind the gold film in the foundation between the Si micro-domes. As shown in figure 2(b), no gold is observed on the side walls of the pillars.

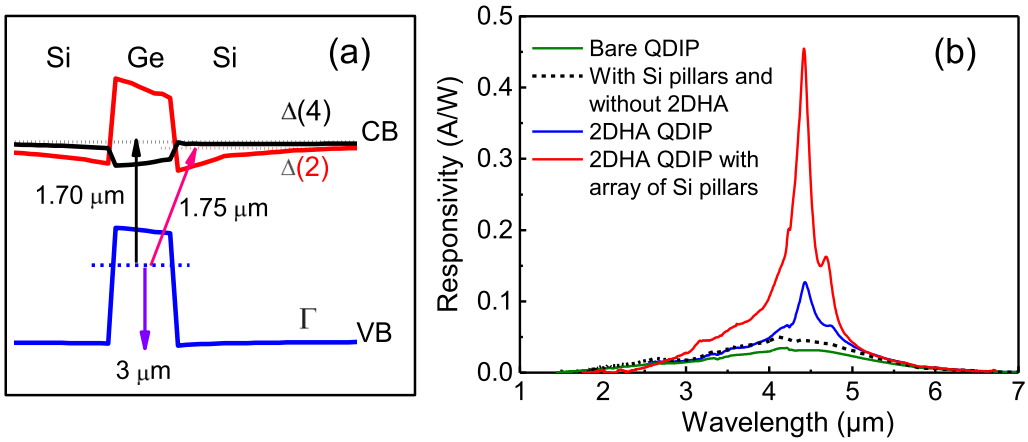

Figure 3. (a) Calculated band-edge diagram of the strained Ge pyramid in Si(001) along the growth axis with the relevant intra- andinterband transitions. The pyramid base is 15 nm and the height is1.5 nm. (b) Spectral photoresponse of (i) the bare QDIP, (ii) the detector coated with only the periodic array of the Si pillars without the gold film, (iii) the QDIP with the gold 2DHA plasmonic structure, and (iv) when the Si pillars are mounted on the 2DHA.

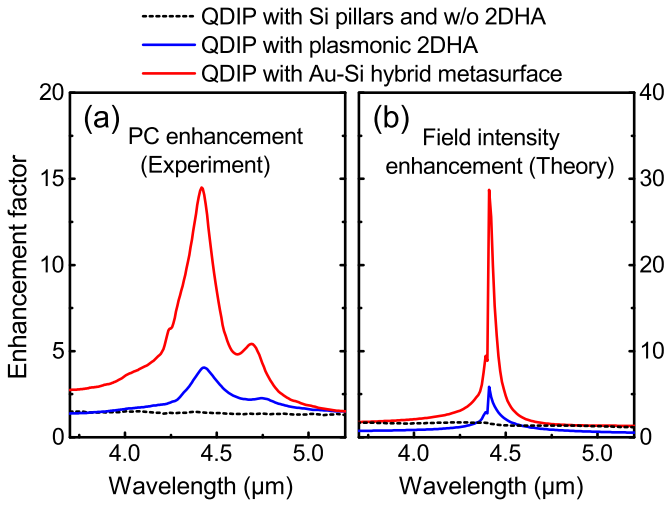

Figure 4. (a) Experimental photoresponse enhancement spectra. (b) Calculated electric near-field intensity enhancement over the quantum dot region.

3. Results and discussion

The energy band-edge diagram of the Ge QD in Si(001) along the growth axis is shown in figure 3(a). The QD is assumed to have a pyramid shape with the base oriented along the [100] and [010] directions. The band structure was calculated using a six-band $\mathbf{k}\cdot\mathbf{p}$ approach for the valence band and a single-band effective-mass approximation for the conduction band, including strain [43, 44]. Due to the tensile strain, the sixfold-degenerate conduction band minimum at the Δ point of Si around the Ge dot splits into the fourfold-degenerate in-plane $\Delta(4)$ valleys and the twofold-degenerate $\Delta(2)$ valleys along the [001] growth direction. In the valence band, there is a large offset and the holes are confined inside the Ge dot at the Γ point. Three types of optical transitions are evident. The mid-IR resonance around 3 μm is associated with the hole intraband transition between the dot ground state and the valence band continuum states. Due to the Ge–Si interface mixing in the real structures, this resonance can shift towards longer wavelengths. The other two near-IR responses at $\lambda \sim 1.7$ μm correspond to the interband transitions between the electrons in the Δ valleys and the holes at the Γ point. In this work, we study the photoresponse of *p*-type GeSi QDIPs. The photocurrent of the devices is generated in the mid-wave atmospheric window and originated from the intraband transitions between the hole states bound inside Ge QDs and continuum or quasi-bound states of the Si matrix. It is worth noting that the mid-IR signal is absent in samples without the presence of Ge dot layers [44]. We thus associate this photoresponse with Ge nanoislands.

The measured responsivity spectra of the devices are shown in figure 3(b). The photoresponse spectra of the reference sample and of the device with the Si micro-domes alone are very similar. The spectral band of the photoresponse covers the wavelength range from 2 to 6 μm with the maximum sensitivity at $\approx$ 4.3–4.5 μm. Compared with a bare QDIP, the detectors coupled with metal and hybrid metasurfaces provide a strong sensitivity enhancement at the wavelength around 4.4 μm. The larger enhancement is observed for the QDIP with a hybrid metal-dielectric structure. The enhancement factor is plotted in figure 4(a). According to the grating equations for a pitch of 1.3 μm [45, 46], both the first-order Au/Si Rayleigh anomaly and the fundamental SP (1,0) (or its degenerate (0,1) mode) resonance are expected at $\approx$4.4 μm. The calculated wavelength is in agreement with the observed position of the dominant responsivity peak. The QDIP coupled with the holey Au film exhibits about 4 $\times$ responsivity enhancement as compared to a bare QDIP and displays about 15 times enhancement when integrated with the hybrid metasurface. Figure 4(a) shows a small secondary peak in photoresponse at 4.7 μm. Previously similar splitting of the SR peak has been observed in long-wave InAs/InGaAs QDIPs at large aperture size [47] and attributed to Bragg scattering

of the counter-propogating Bloch waves in a periodic grating [48, 49]. At normal incidence, the two modes are degenerate under empty lattice approximation or for infinitely small holes. The modes split as the diameter of the hole increases so that an energy gap becomes evident.

The difference between the RA and SP excitation can be seen in the electric near-field distribution in the vicinity of grating surfaces. For RAs, the field enhancement extends far from the metal-dielectric interface, whereas, for SPs, the field intensity decreases exponentially with the distance from the grating [21, 50]. To get insight into the SPs and other resonant features, we inspect how the actual electric fields near the metal surfaces change. The near-field components distributions are calculated with the 3D finite-element frequency-domain method based commercial software COMSOL Multiphysics by numerically solving the Maxwell equations. Floquet periodic boundary conditions were used along the planar x and y-directions to simulate an infinite array of unit cells. Perfectly matched layers were used along the vertical direction (z-direction) to prevent the reflection of the waves from the top and bottom domain boundaries. The plane-wave radiation with a circular polarization falls normally on the top of the QDIPs. We use the frequency-dependent dielectric function of the gold from the study by Rakić *et al* [51], and the refractive index of Si is taken to be 3.42 [52]. The near-field intensity enhancement factor is quantified by dividing the field intensity integrated over the QD active region $\int_V |E|^2 dV$ by that in the bare sample. The calculated enhancement spectra are shown in figure 4(b). The spectral positions of the simulated field intensity enhancement and the experimental responsivity enhancement agree well with each other. A significant difference is the broadening in the experimental spectra. The much broader bandwidth of the measured photoresponse enhancement spectra is probably due the fluctuations of the sizes and shapes of the holes and Si pillars.

Figure 5 shows the color maps of the electric near-field intensity at the resonance wavelength of 4.4 μm for different types of metasurface on top of Ge/Si QDIPs. The horizontal white dashed lines in the figure indicate the QD active region. The yellow rectangles are the cross sections of the gold film. The near-field distribution for the Si pillar without the gold film is found to concentrate at the sides of the slab (figure 5(a)) and arises from the Mie-like scattering. No noticeable field enhancement is observed in the region occupied by QDs. For the QDIP coupled with the perforated gold film, the most intense electric fields are localized at the edge of the hole and correspond to the excitation of the evanescent surface mode on the Au-Si interface (figure 5(b)). The RA with a lower field intensity is present at distances where the plasmonic fields have significantly decayed, and looks like a propagating plane wave with infinite extent [50, 53]. In figure 5(c), we see that filling the periodic hole array with Si pillars has a crucial effect on the field distribution. The resulting electric fields are not a simple superposition of the near-field components for the 2DHA and Si pillar structures alone, implying antenna-like coupling between the plasmonic and dielectric elements. The SPs become less pronounced, and a surface diffracted wave dominates. Since both the plasmonic and Rayleigh waves

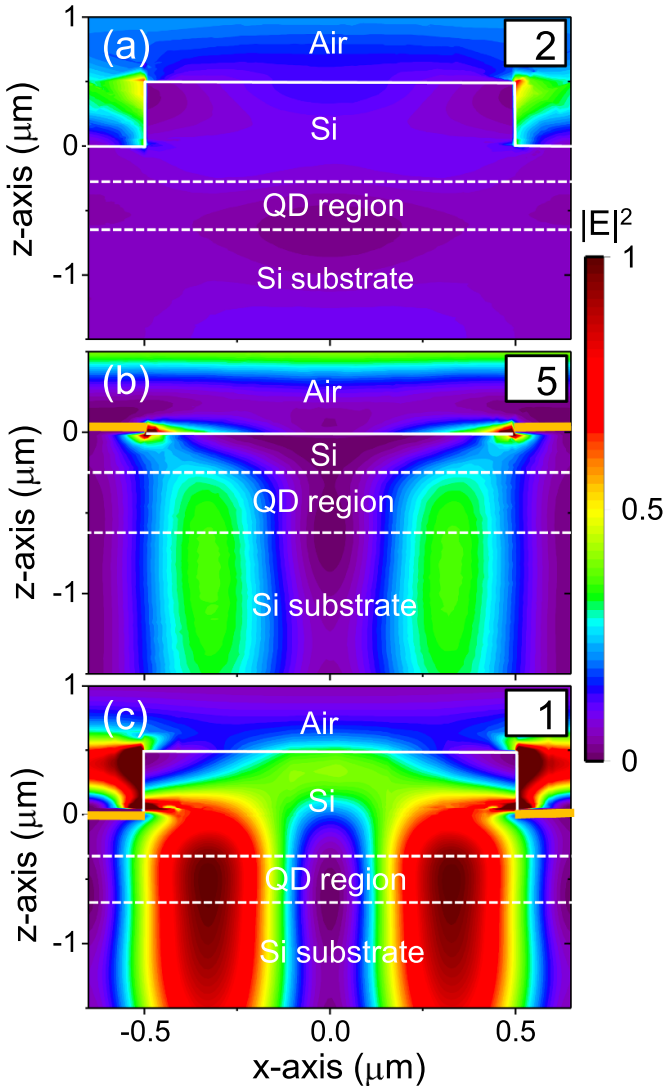

Figure 5. Simulated near-field images of the intensity distribution in the $x-z$ plane at 4.4 μm for (a) a Si pillar array alone, without gold layer, (b) a 2DHA-QDIP structure, and (c) a Si pillar array with the gold film residing between pillars. The light approaches at normal incidence from the top. The cross section of the gold film is shown as yellow boxes. The hole is centered at the origin. The Si boundaries are outlined in white. The active region of Ge quantum dots is between the white dashed lines. The normalized field intensities are scaled by 2 and 5 for (a) and (b), respectively, for the same intensity scale bar.

travel exactly along the QD layers, they can efficiently interact with the dots and increase the QDIP photoresponse. A higher electric field in the QD region of the QDIP coupled with the hybrid metal-dielectric metasurface results in a significant photoresponse improvement, compared to when all-dielectric and metal gratings work separately (figure 4(b)). We believe that this problem deserves further in-depth theoretical analysis.

Let us analyse the experimental transmittance spectra shown in figure 6. Frequently, the enhanced transmission of metallic 2DHA structures is discussed in terms of a Fano-type interference between the discrete plasmon resonance and the non-resonant radiative damping of plasmons [54–57]. A

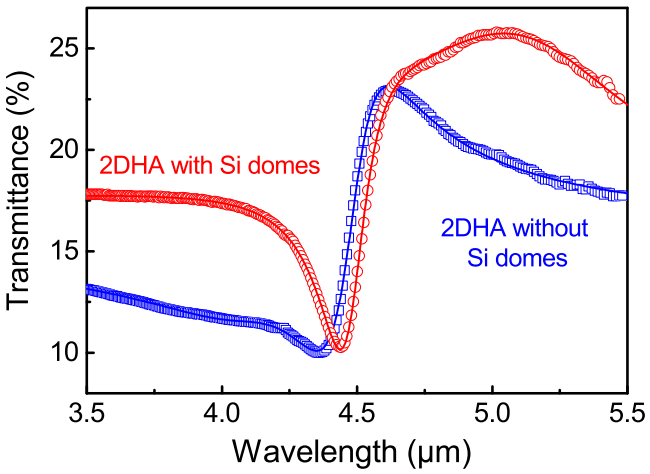

Figure 6. Experimental transmittance spectra (symbols) and the best-fits to the Fano-type lineshape (equation (1)) (lines) of the QDIPs with the gold 2DHA plasmonic structure and when the Si pillars are mounted on the 2DHA (hybrid metal-dielectric metasurface).

Rayleigh-like scattering of SPs by the 2DHAs is supposed to be the microscopic origin of this dumping [56]. The spectral overlapping of the first-order RA with the SP resonance would lead to the generation of a coupled RA–SP mode. In this case, the Fano-type resonance is expected to arise from the interference between RA and SPs, supported by the holey gold film [58]. The transmission is then expected to be of the form [55]

$$T = T_d + |t|^2 \frac{[\epsilon + q]^2}{1 + \epsilon^2}, \qquad (1)$$

where T_d is related to the direct light penetration, $|t|^2$ is the non-resonant transmission coefficient, ε is the detuning from the resonance given by $\epsilon = [\omega - (\omega_0 + \Delta)]/(\Gamma/2)$, ω_0 is the resonant frequency, Δ is the resonant shift, Γ is the linewidth, $\pi q^2/2$ defines the ratio between the resonant and non-resonant transition amplitudes [59]. The solid lines in figure 6 show the curve fitting of the experimental transmittance spectra using equation (1) with the fitting parameters of $q_1 = -1.1 \pm 0.1$ ($\pi q_1^2/2 \simeq 1.9$) and $q_2 = -0.4 \pm 0.1$ ($\pi q_2^2/2 \simeq 0.3$) for the 2DHA QDIP and for the detector integrated with a hybrid optical antenna, respectively. Clearly, the transmittance profiles agree well with the Fano-type interference model, considering that no dependence of the coupling parameter q on wavelength is taken into account. Reduction of the $|q|$ parameter by filling the 2DHA with Si pillars implies the increase of the Rayleigh-like non-resonant scattering of light from the Si micro-domes, yielding the light to get more coupled to the 2DHA RA.

4. Conclusions

In summary, we study a metal-dielectric coupling system integrated with a mid-infrared Ge/Si quantum dot photodetector. The composite metasurface consists of a two-dimensional regular array of silicon pillars protruding through subwavelength holes in a periodically perforated gold film on top of the detector active region. The hybrid device exhibits about four times photoresponse enhancement, as compared to the QDIP with the top 2DHA gold plasmonic structure without the Si micro-domes, and displays about 15 times peak responsivity enhancement at a wavelength of 4.4 μm relative to the bare detector. Simulation of the spatial near-field distribution demonstrates that a diffracted wave related to the Rayleigh anomaly dominates the enhanced electromagnetic field near the Si-Au interface, which means that a higher proportion of the field has access to the limited absorption QD layer thickness.

Acknowledgments

The authors thank V A Armbrister for the MBE growth. The study was supported by the Russian Foundation for Basic Research (Project No. 16-29-03024). The part of the work associated with numerical simulation of the near-field components was also supported by State Program No. 0306-200019-0019. The electron-beam lithography was performed in the Analytical and Technological Research Center at Physics Department of Novosibirsk State University.

ORCID iD

Andrew Yakimov https://orcid.org/0000-0002-6141-427X

References

[1] Lee S C, Krishna S and Brueck S R J 2010 *Appl. Phys. Lett.* **97** 021112
[2] Chang C C, Sharma Y D, Kim Y S, Bur J A, Shenoi R V, Krishna S, Huang D and Lin S Y 2010 *Nano Lett.* **10** 1704–9
[3] Liu R, Vasinajindakaw P, Gu G, Vaillancourt J and Lu X 2013 *J. Phys. D: Appl. Phys.* **46** 015102
[4] Gu G, Vaillancourt J, Vasinajindakaw P and Lu X 2013 *Semicond. Sci. Technol.* **28** 105005
[5] Zhang Y, Vaillancourt J, Gu G, Guo W and Lu X 2016 *J. Appl. Phys.* **119** 193103
[6] Yakimov A I, Kirienko V V, Bloshkin A A, Armbrister V A and Dvurechenskii A V 2017 *J. Appl. Phys.* **122** 133101
[7] Yakimov A I, Kirienko V V, Bloshkin A A, Armbrister V A, Dvurechenskii A V and Hartmann J M 2017 *Opt. Express* **25** 25602
[8] Yakimov A I, Kirienko V V, Armbrister V A, Bloshkin A A and Dvurechenskii A V 2018 *Appl. Phys. Lett.* **112** 171107
[9] Ebbesen T W, Lezec H J, Ghaemi H F, Thio T and Wolf P A 1998 *Nature* **391** 667–9
[10] Ghaemi H F, Thio T, Grupp D E, Ebbesen T W and Lezec H J 1998 *Phys. Rev.* B **58** 6779–82
[11] Genet C and Ebbesen T W 2007 *Nature* **445** 39–46
[12] Law S, Podolskiy V and Wasserman D 2013 *Nanophotonics* **2** 103–30
[13] Tang W X, Zhang H, Ma H, Jiang W and Cui T 2019 *Adv. Optical Mater.* **7** 1800421
[14] Pendry J B, Martin-Moreno L and Garcia-Vidal F J 2004 *Science* **305** 847
[15] Garcia-Vidal F J, Martin-Moreno L and Pendry J B 2005 *J. Opt. A: Pure Appl. Opt.* **7** S97

[16] Pors A, Moreno E, Martin-Moreno L, Pendry J B and Garcia-Vidal F J 2012 *Phys. Rev. Lett.* **108** 223905
[17] Khurgin J B 2017 *Phil. Trans. R. Soc.* A **375** 20160068
[18] Hessel A and Oliner A 1965 *Appl. Opt.* **4** 1275
[19] Maradudin A A, Simonsen I, Polanco J and Fitzgerald R M 2016 *J. Opt.* **18** 024004
[20] McMahon J, Henzie J, Odom T W, Schatz G C and Gray S K 2007 *Opt. Express* **15** 18119
[21] Gao H, McMahon J, Lee M, Henzie J, Gray S, Schatz G and Odom T 2009 *Opt. Express* **17** 2334
[22] Krasnok A E, Miroshnichenko A E, Belov P A and Krishar Y S 2012 *Opt. Express* **20** 20599
[23] Moitra P, Slovick B, Ya Z G and Krishnamurthy S 2014 *Appl. Phys. Lett.* **104** 171102
[24] Jahani S and Jacob Z 2016 *Nat. Nanotechnol.* **11** 23
[25] Genevet P, Capasso F, Aieta F, Khorasaninejad M and Delvin R 2017 *Optica* **4** 139
[26] Decker M and Staude I 2016 *J. Opt.* **18** 103001
[27] Kamali S M, Arbabi E, Arbabi A and Faraon A 2018 *Nanophotonics* **7** 1041
[28] Liu M, Fan Q, Yu L and Xu T 2019 *Opt. Express* **27** 10738
[29] Ahn W, Boriskina S, Hong Y and Reinhard B 2012 *ACS Nano* **6** 951
[30] Xiao Y F, Liu Y C, Li B B, Chen Y L, Li Y and Gong Q 2012 *Phys. Rev.* B **85** 031805
[31] Jiang R, Li B, Fang C and Wang J 2014 *Adv. Mater.* **26** 5274
[32] Guo R, Rusak E, Staude I, Dominguez J, Decker M, Rockstuhl C, Brener I, Neshev D and Kivshar Y 2016 *ACS Photonics* **3** 349
[33] Decker M, Pertsch T and Staude I 2018 *Phil. Trans. R. Soc.* A **375** 20160312
[34] Giudicatti S, Marabelli F, Valsesia A, Pellacani P, Colpo P and Rossi F 2012 *J. Opt. Soc. Am.* B **29** 1641–7
[35] Liu R, Zhao X, Roberts C, Yu L, Mohseni P K, Li X, Podolskiy V and Wasserman D 2016 *Adv. Mater.* **28** 1441
[36] Kumar R and Ramakrishna S A 2018 *J. Phys. D: Appl. Phys.* **51** 165104
[37] Tan C L and Mohseni H 2018 *Nanophotonics* **7** 169–97
[38] Yakimov A I, Mikhalyov G Y, Dvurechenskii A V and Nikiforov A I 2007 *J. Appl. Phys.* **102** 093714
[39] Yakimov A I, Kirienko V V, Armbrister V A, Bloshkin A A and Dvurechenskii A V 2014 *Phys. Rev.* B **90** 035430
[40] Yakimov A I, Kirienko V V, Armbrister V A, Bloshkin A A and Dvurechenskii A V 2015 *Appl. Phys. Lett.* **107** 213502
[41] Yakimov A I, Kirienko V V, Armbrister V A, Bloshkin A and Dvurechenskii A V 2016 *Mater. Res. Express* **3** 105032
[42] Finkman E, Shuall N, Vardi A, Le Thanh V and Schacham S E 2008 *J. Appl. Phys.* **103** 093114
[43] Yakimov A I, Timofeev V A, Bloshkin A A, Kirienko V V, Nikiforov A I and Dvurechenskii A V 2012 *J. Appl. Phys.* **112** 034511
[44] Yakimov A, Nikiforov A, Bloshkin A and Dvurechenskii A 2011 *Nanoscale Res. Lett.* **6** 208
[45] Minhas B K, Fan W, Agi K, Brueck S and Malloy K 2002 *J. Opt. Soc. Am.* A **19** 1352–9
[46] Kim T J, Thio T, Ebbesen T, Grupp D and Lezec H 1999 *Opt. Lett.* **24** 256–8
[47] Lee S, Kang J, Park Q H, Krishna S and Brueck S 2016 *Sci. Rep.* **6** 24400
[48] Barnes W, Preist T, Kitson S, Sambles J, Cotter N and Nash D 1995 *Phys. Rev.* B **51** 11164
[49] Kitson S, Barnes W, Bradberry G and Sambles J 1996 *Appl. Phys. Lett.* **79** 7383–5
[50] Steele J, Moran C, Lee A, Aquirre C and Halas N 2003 *Phys. Rev.* B **68** 205103
[51] Rakić A D, Djurišić A B, Elazar J M and Majewski M L 1998 *Appl. Opt.* **37** 5271–83
[52] Salzberg C D and Villa J J 1957 *J. Opt. Soc. Am.* **47** 244–6
[53] Chang S H, Gray S and Schatz G 2005 *Opt. Express* **13** 3150
[54] Sarrazin M, Vigneron J and Vigoureux J 2003 *Phys. Rev.* B **67** 085415
[55] Genet C, van Exter M P and Woerdman J P 2003 *Opt. Commun.* **225** 331–6
[56] Kim D *et al* 2003 *Phys. Rev. Lett.* **91** 143901
[57] Vasinajindakaw P, Vaillancourt J, Gu G, Liu R, Ling Y and Lu X 2011 *Appl. Phys. Lett.* **98** 211111
[58] Shen Y *et al* 2013 *Nat. Commun.* **4** 2381
[59] Fano U 1961 *Phys. Rev.* **124** 1866